TOWARDS A EUROPEAN HELICOPTER NOISE CALCULATION METHOD

Marthijn Tuinstra, Jos Stevens, NLR – Netherlands Aerospace Centre (Netherlands)

Nico van Oosten, Anotec Engineering (Spain)

Herold Olsen, SINTEF (Norway)

Abstract

Helicopter noise is strongly dependent on flight conditions, exhibiting in addition a pronounced directivity, complicating noise modelling. In land-use planning, the current best practice stems from fixed-wing aircraft and follows a Noise Power Distance approach that is unsuitable to include these features. The European Commission commissioned the development a novel helicopter noise model to be eventually part of a public "European Environmental Model Suite for Aviation". The model embodies a helicopter noise calculation method based on the current state-of-the-art. A clustering strategy has been used to represent the European helicopter fleet, thus avoiding the need for performing noise measurements on all types of helicopters. The method uses an empirical source model, with noise hemispheres to faithfully describe the noise directivity pattern. Emission characteristics of a helicopter type are described by a set of hemispheres measured for a range of conditions within the flight envelope. Atmospheric propagation effects are accounted for to evaluate the noise hindrance experienced on-ground. The latter is based on established public models for atmospheric propagation, ground reflection and surface impedance.

1. INTRODUCTION

1.1. Background

Helicopter noise emission is strongly dependent on flight conditions and varies heavily with emission angles. Currently used land-use planning methods in Europe were developed for fixed wing aircraft (ECAC Doc 29[1]) and are recognized not to be able to represent helicopter noise with sufficient fidelity. To fill such a gap the European Commission commissioned the development of a European approach to helicopter noise modelling suited to support END monitoring activities. In view of ensuring its fitness-for-purpose it was further required that the method should match ICAO Doc 9911 & ECAC Doc 29 in complexity and sophistication while being able to account for a mixed fleet of helicopters. The final aim was to replicate with high fidelity the noise of a given helicopter type, providing a robust alternative to the fixed-wing aircraft approach of ECAC Doc 29 in terms of Sound Exposure Level (SEL), Effective Perceived Noise Levels (EPNdB) or Maximum A-weighted Noise Levels ($L_{A,max}$). An overview of this work is provided in a companion paper by Tuinstra et al.[2]

1.2. Approach

The objective was to provide a method allowing the prediction of noise levels for a passing helicopter targeting the most common types within the European helicopter fleet. The method starts by considering the noise levels at an observer location $\mathbf{x}$, the latter being a function of the time dependent helicopter location $\mathbf{y}(t)$ and centre frequency f_c :

$$L_o(f_c, \mathbf{x}, \mathbf{y}(t)) = L_{i,j} + \Delta L_p \quad (1)$$

The observer noise level is decomposed in a source term $L_{i,j}$ and a scaling factor to account for atmospheric propagation ΔL_p. The latter term comprises those effects relating to spherical spreading, atmospheric attenuation and ground absorption effects.

For an accurate source description of a given helicopter type, the method relies on sets of measured noise hemispheres, covering the relevant conditions in the flight envelope. Noise hemispheres are provided in one-third octave bands, from which SEL, EPNdB, $L_{A,max}$ and other noise metrics can be derived. To allow

Presented at 44th European Rotorcraft Forum, Delft, The Netherlands, 19-20 September, 2018

representation of a large portion of the European helicopter fleet based on a limited noise database, helicopter types with similar noise characteristics were clustered together within a single class. In the source term $L_{i,j}$, i and j are, respectively, the helicopter class index and time dependent flight condition index.

2. FLEET MODEL

To derive a list of the civil helicopters active in 'Europe', use has been made of the Rotorspot online database[3] – a worldwide repository of all registered and de-registered civil helicopters. Evolving from a private initiative this database includes official aircraft registry records, enhanced with information from various other sources, including manufacturers. The information that it provides goes well beyond the official registry records – notably flagging helicopters that albeit still registered are known to be non-operational (e.g. due to an accident). Using the Rotorspot data set of late December 2014, circa 350 different helicopter types/variants were identified from the total 7400 individual registrations. By assigning the ICAO Aircraft Type Designators (ATD's)[4] variants of a single helicopter type were subsequently grouped together, eventually reducing the list to 92 different helicopter types[*].

Detailed configuration data and noise level information was hence collected for these helicopter types. Table 1 gives an overview of the parameters considered, which are known to influence noise levels and noise characteristics. The relevant data was collected from several sources[5,6,7,8] - with reference noise levels gathered from both an EASA database[9] and the German Luftfahrt-Bundesamt database[10]. Noise data is available for about 40% of helicopter types, representing more than 80% of the total number of active helicopters in the European fleet. This sort of data is however lacking notably for older types, for Russian designs and for homebuilt/ultralight helicopters.

Based on results of previous work carried out for EASA (EHEST) and the European Commission (CLEANSKY), estimates for both the annual number of Flight Hours (FHs) and the average number of take-offs/landings per flight hour were calculated. The calculation assumed a number characteristic operations for each specific helicopter type in accordance to the classification of Table 2. The latter is based on both previous experience and expert judgement. Certain helicopter types can be used for a combination of operations - for example a Robinson R44 can be used for 'Private', 'Training' and 'Rental' while a Sikorsky S-92 can be used for Commercial Air Transport (CAT) and Utility (e.g. Search and Rescue operations). Different variants of a specific helicopter type can also be used for different types of operation - for example, whilst the Super Puma AS332L variants are mainly used for CAT and State Flights, the Super Puma AS332C variants are mainly used for Utility. This is reflected in the assigned operations.

For each operation and combinations thereof, estimates for both the annual number of flight hours per helicopter and the average number of take-offs/landings per flight hour per helicopter were appraised. To cater for the fact that helicopter types assigned to (a combination of) operations will not fly the same number of flight hours – e.g. in CAT the offshore transport helicopters will fly more hours than the helicopters used for onshore transport duties - variants on the types of operations were also considered. Figure 1 gives an overview of all combinations used in this study.

The assessment shows that the combined European helicopter fleet per year performs circa 2.5 million flight hours and 6.6 million take-offs/landings. To enable verification of the soundness of the aggregate values, the number of flight hours has been compared with available Canadian data[11] as flight hours flown in Canada are part of the Annual Airworthiness Information Report. In 2007, the Canadian civil helicopter fleet consisted of 2263 helicopters which flew a total of 0.79 million flight hours (FH). This implies an average of about 349 FHs/year/helicopter. Comparable metrics for the European fleet (in 2014) amount to 337 FHs/year/helicopter, comparing well with the Canadian average.

Helicopter types of similar configuration and certification noise levels were combined in a single class as denoted in Table 3. To select the most relevant classes for inclusion in the noise model these were ranked by: (i) the total number of helicopters per class (ii) the total number of flight hours per class per year; and (iii) the total number of take-offs and landings per class per year. The premise is that noise hindrance caused by a specific helicopter type relates directly to these parameters. The set of helicopter classes that include Robinson 44, Robinson 22, Aerospatiale 350 Ecureuil, Bell 206 JetRanger, Schweizer 269, Eurocopter 135, Agusta 109 and Eurocopter 120B when aggregated together represent circa 77% of the total number of helicopters, 70% of the total number of flight hours per year and 87% of the total number of take-offs/landings per year.

[*] From here on, when type is mentioned type and variants on this helicopter type is implied

Presented at 44th European Rotorcraft Forum, Delft, The Netherlands, 19-20 September, 2018

Table 1 Parameter overview of collected configuration data and noise level information

Parameter	Explanation
Maximum Take-Off Weight [kg]	
Main rotor number of blades	
Main rotor direction of rotation (viewed from above)	CW = Clockwise, CCW = Counter-Clockwise, Co-ax = Coaxial rotors, Intermesh = intermeshing rotors
Tail rotor number of blades	
Tail rotor position	L = Left, R = Right, in fin = Fan-in-fin, NOTAR = No Tail Rotor
Engine type	P = Piston, T = Turbine
Engine number	
ICAO noise level, take-off [EPNdB]	for Chapter 8 helicopters
ICAO noise level, overflight[EPNdB]	for Chapter 8 helicopters
ICAO noise level, approach[EPNdB]	for Chapter 8 helicopters
ICAO noise level, overflight [dBA]	for Chapter 11 helicopters

Table 2 Characteristic types of operation

Type of operation	Description
Agriculture	Specialised operations specifically for agricultural purposes, e.g. crop spraying
CAT	Commercial Air Transport
Exec	Executive transport
HEMS	Helicopter Emergency Medical Services
Maintaining airworthiness	A limited number of annual flights with the main objective to maintain the helicopter type in terms of airworthiness and pilot's currency (type rating)
Private	Leisure flights in which it is assumed that the pilot is also the owner of the helicopter
Rental	Flights in which the helicopter is rented for photo flights, A to B flights, recreational flights, etc.
State	Flights with state aircraft and/or for police or fire fighting purposes
Training	Flights for training purposes
Utility	All other forms of specialised operations (former Aerial Work)

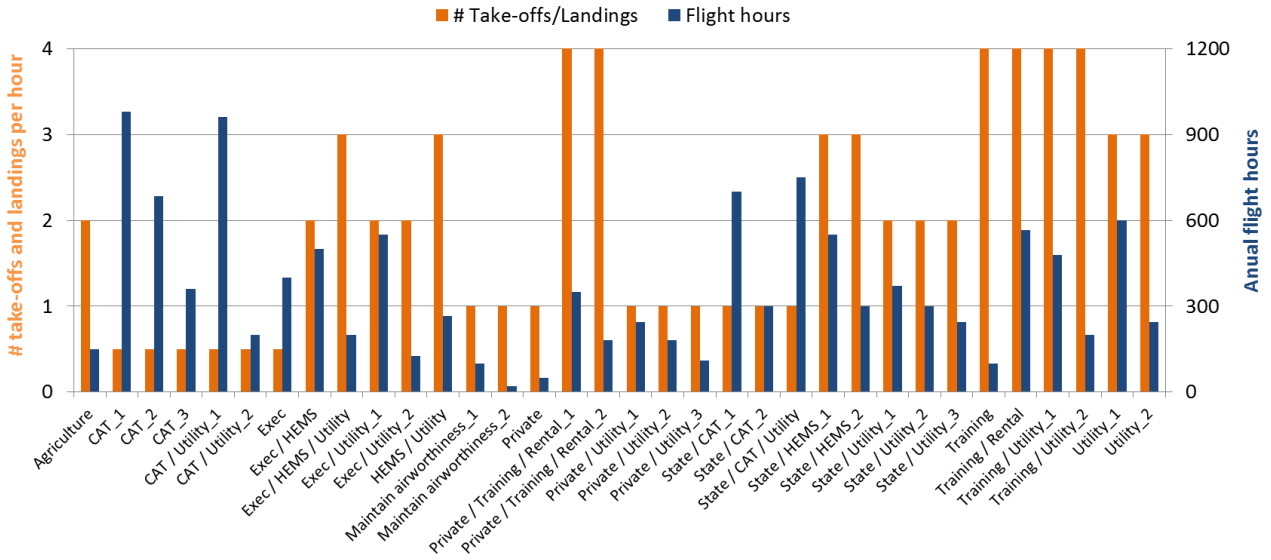

Figure 1 Average number of take-off and landings per hour and annual flight hours per (combination of) operation type and variant

Presented at 44th European Rotorcraft Forum, Delft, The Netherlands, 19-20 September, 2018

Table 3 Helicopter classes containing more than one helicopter type, types within square brackets denote geometricaly mirrored configurations

Helicopter class	ATD	Included helicopter types
Agusta A109	A109	A109, B105, B427, B429, BK17, EC45
AgustaWestland AW189	A189	A189, A149, [EC75]
AS332 Super Puma	AS32	AS32, AS3B
AS350 Ecureuil	AS50	AS50, ALO2, ALO3, LAMA, PSW4
AS355 Ecureuil 2	AS55	AS55, MI2
AS365 Dauphin 2	AS65	AS65, EC55
Bell 206 JetRanger	B06	B06, B06T, B47T, H12T, R66
Bell 212	B212	B212, B222, B230
Bell 412	B412	B412, B430, S76
Bell UH-1 Iroquois	UH1	UH1, HUCO
Dynali H2	DYH2	DYH2, [ULTS], plus a number of homebuilts like Dynali H3, Rotorsmart HeliSmart, [Ultrasport 331]
EC120 Colibri	EC20	EC20, EC30, GAZL
EC135	EC35	EC35, EC145T2
EC225 Super Puma	EC25	EC25, MI8
Enstrom 480	EN48	EN48, S330
Famà Kiss 209	K209	K209, B150, [ES11], [EXEJ]
PZL-Swidnik W-3 Sokol	W3	W3, PUMA
Robinson 22	R22	R22, CH7, V500, [A600], [BABY], [DRAG], [EXEC], [SCOR], plus a number of homebuilts like EliSport CH-77 Ranabot, Cicaré CH-7T Spirit Tandem, BHR Mustang F260N, BHR Mustang F290, Hungarocopter HC-01, Italian Rotors T22, BHR Fandango F360, [LCA Helicopter LH212]
Robinson 44	R44	R44, B47G, B47J, ELTO, UH12
Schweizer 300	H269	H269, BRB2, EN28, [ZA6]

Table 4 Ranking of helicopters classes, including noise relevant configuration characteristics

Class	MTOW [kg]	MR # blades	MR direction of rotation	Tail rotor # blades	Tail rotor position	Engine type	Engine #	ICAO An. 16 Ch.8 Take Off [EPNdB]	ICAO An. 16 Ch.8 Overflight [EPNdB]	ICAO An. 16 Ch.8 Approach [EPNdB]	ICAO An.16 Ch. 11 [dBA]
R44†	943-1340	2	CCW	2	L*	Piston	1				80.9-82
R22†	310-680	2	CCW	2	L	Piston	1	80.2-84.2	81.3-82.0	86.7	76.9-78.9
AS50†	1497-2250	3	CW	2*	R	Turbine	1	89.7-90.1	87.2-87.6	91.2-91.4	84.4-85.4
B06†	1225-2019	2	CCW	2	L*	Turbine	1*	87.4-89.2	84.5-87.8	87.8-92.5	85.0
H269†	650-1179	3	CCW	2	L*	Piston	1	89.0-91.0	81.0-83.0	91.0-93.0	78.8-81.2
EC35†	2720-3700	4	CCW	10	in fin	Turbine	2	88.3-88.6	84.0-85.7	90.3-94.9	80.2-81.4
A109	2300-3585	4	CCW	2*	L	Turbine	2	88.0-92.9	87.2-91.9	90.1-96.1	
EC20†	1715-2500	3	CW	8*	in fin	Turbine	1	85.5	84.2	90.5	78.7-81.1
B412†	4082-5400	4	CCW	4*	L*	Turbine	2	91.4-96.0	89.8-95.7	93.1-97.7	
A139	6800	5	CCW	4	R	Turbine	2	90.3	90.7	94.1	
AS32	8600-9300	4	CW	5*	R	Turbine	2	91.8-94.3	90.5-93.5	94.5-96.1	
S92	12020	4	CCW	4	R	Turbine	2	94.6	97.2	97.5	

* This is the most occurring configuration; however variants exist with a different configuration

† For these helicopter classes noise databases were established, see Tuinstra et al.[2]

Presented at 44th European Rotorcraft Forum, Delft, The Netherlands, 19-20 September, 2018

The statistics also show that the set { Bell 412, AgustaWestland 139, Aerospatiale 332 Super Puma and Sikorsky 92 } includes the most active heavier helicopter types in the European helicopter fleet - covering 6% of the total number of helicopters, 14% of the annual flight hours and 3% of the take-offs and landings. Although these helicopters types are responsible for only a small fraction of the European helicopter fleet operations the associated emitted noise levels are high and can be expected to create significant noise hindrances.

An overview of the aforementioned classes and associated characteristics is provided by Table 4. In the framework of this project, detailed noise databases were acquired for eight helicopter types.

3. SOURCE MODEL

3.1. Noise hemispheres

A hemisphere approach was followed to describe the source of helicopter noise. This follows the approach elicited by next-generation helicopter noise models (HELENA[12], AAM[13] and SELENE[14]) as hemispheres provide an adequate manner to describe the complex and highly directive nature of helicopter noise phenomena. Notwithstanding this fact, it is noteworthy that noise measurements for the purpose of hemisphere derivation should be performed with great care, and generally follow the guidelines given in ICAO Annex 16.

Hemisphere noise levels were defined at a fixed reference distance of 60m and included effects of atmospheric absorption under ICAO atmospheric reference conditions. This distance matches that used for the frequency extrapolation method outlined in Doc 9501[15]. The latter was used to reconstruct masked one-third octave bands levels above 2 kHz, assuming a flat spectrum (equal energy) following the last good band. Hemispheres were composed of one-third octave bands, for frequencies between 10Hz (10th band) to 10kHz (40th band).

Hemispheres are defined as function of azimuth φ and polar angle θ, binned in intervals of 10 degrees. The emission angles are related to Cartesian coordinates in the aircraft body axis system as follows:

$$\begin{aligned} x &= r_h \cos\theta \\ y &= r_h \sin\theta \sin\varphi \\ z &= r_h \sin\theta \cos\varphi \end{aligned} \tag{2}$$

in which $-90° \le \varphi \le 90°$ and $0° \le \theta \le 180°$.

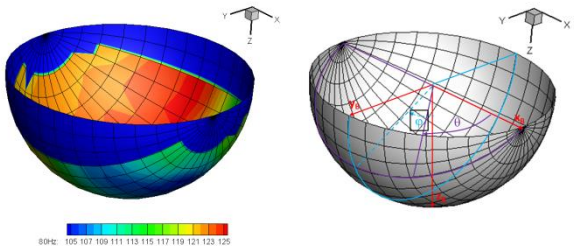

Figure 2 Example of a noise hemisphere (left), based on measurements of a R22 helicopter, 80Hz 1/3 octave band frequency, given in aircraft body axis system(right)

Negative and positive azimuth angles correspond, respectively, to port and starboard of the helicopter. For polar angles $\theta < 90°$ noise emits in the forward direction and for $\theta > 90°$ in the rearward direction of the helicopter (see figure 2).

The example hemisphere shows that its surface is not filled entirely with noise data. For both practical reasons and data quality-related issues, hemisphere data is required to cover at least the following emission angles:

$$\begin{aligned} -60° \le \varphi \le 60° \\ \theta_{t1} \le \theta \le \theta_{t2} \end{aligned} \tag{3}$$

where θ_{t1} and θ_{t2} correspond to the polar angles at 10dB down time instance. Measurement of higher lateral angles is deemed impractical, as it requires flat open terrains exceeding 1km or complex measurement setups[16,17]. In such cases, data quality cannot be ensured due to the long distance, propagation near parallel to the surface and relatively low helicopter noise levels when compared with the background noise. Following a similar reasoning, only polar angles that lie within the 10dB-down-period (based on EPNL) are eventually considered.

To obtain source levels from stored hemispheres, a bilinear interpolation is applied as follows

$$\tilde{L}_h(f_c,\varphi,\theta)_{i,j} = 10\log_{10}\left(\begin{bmatrix} \frac{\varphi^{m+1}-\varphi}{\Delta\varphi} & \frac{\varphi-\varphi^{m}}{\Delta\varphi} \end{bmatrix} \begin{bmatrix} 10^{\frac{L_h(f_c)_{i,j}^{m,n}}{10}} & 10^{\frac{L_h(f_c)_{i,j}^{m,n+1}}{10}} \\ 10^{\frac{L_h(f_c)_{i,j}^{m+1,n}}{10}} & 10^{\frac{L_h(f_c)_{i,j}^{m+1,n+1}}{10}} \end{bmatrix} \begin{bmatrix} \frac{\theta^{n+1}-\theta}{\Delta\theta} \\ \frac{\theta-\theta^{n}}{\Delta\theta} \end{bmatrix} \right) \tag{4}$$

in which m and n are the azimuth and polar index respectively, with $\varphi^m < \varphi < \varphi^{m+1}$ and $\theta^n < \theta < \theta^{n+1}$. When exceeding the range for which data is available, constant value extrapolation should be applied from the nearest filled data bin. The nearest bin is given by the subset of indices for which $\delta_{m,n}$ is minimized:

$$\arg\min_{m,n}\left\{\delta_{m,n}\right\} \tag{5}$$

Presented at 44th European Rotorcraft Forum, Delft, The Netherlands, 19-20 September, 2018

In this $\delta_{m,n}$ is the absolute angle between a bin and target value φ,θ, defined by:

(6) $$\delta_{m,n} = \cos^{-1}\left(\mathbf{x}(\varphi,\theta)\cdot\mathbf{x}_{m,n}\right)$$

The vectors $\mathbf{x}$ and $\mathbf{x}_{m,n}$ are given by eq. (2), with r_h=1. In case there are multiple closest bins, the energetic average of the closest bins is taken.

3.2. Flight conditions

The helicopter noise source is described by a set of hemispheres covering a range of flight conditions relevant to noise emission, which is characterised by both airspeed and rate of descent/climb. Until an adequate method will be established, interpolation between noise hemispheres representing different flight conditions is not possible and the recommended practice is to reconstruct flight paths using existing flight conditions in the hemisphere data base.

Figure 3 shows a diagram with the impulsive noise boundaries as function of airspeed and Rate of Climb/Descent for the UH-1 helicopter. Two areas can be identified: (i) an area related to Blade Vortex Interaction (BVI) that occurs mainly for descending flight; (ii) another area associated with high-speed impulsive noise, which occurs when the helicopter is in fast forward flight. Although the exact location of their boundaries will vary depending on helicopter type, this diagram is applicable to any helicopter. An example of the impact on noise emission is shown in figure 4, presenting maximum A-weighted sound pressure levels as function of climb- and airspeed for the EC130 helicopter. A difference of up to 15dB in noise levels is observed over the covered flight envelope. A second observation is that the noise levels vary little (generally within 1dB) as function of rate of climb.

Figures 3 and 4 enable to conclude that, for descents, helicopter noise will vary strongly depending on airspeed and descent angle. This condition should be reflected in the hemisphere data set. Usage of angle variations of 3 degrees and of at least 4 different velocities over the operational range is therefore recommended. The climb region is sufficiently covered by considering a number of climb angles, e.g. 3, 6 and 9 degrees, at the best rate of climb speed (V_y). It is also suggested to: (i) include the maximum climb angle as stated in the aircraft flight manual; (ii) keep level flight conditions at 90% of the speed at level flight for maximum continuous power (V_H) and +10kts (or V_H whichever is the smallest), -15kts and -30kts increments on 0.9 V_H.

The above recommendations should merely serve as guidelines. For each helicopter type to be included in the model the test matrix should be tailored for the specific type, allowing for the potential adaptations to best reflect its actual operational envelope. An example of the noise measurement point distribution for the EC120 is given in figure 5.

3.3. Helicopter type

A clustering into classes was adopted to model the European helicopter fleet. In case a helicopter type is modelled for which a noise database was established for another helicopter within its class, or when no noise database is established for its class at all, this needs further consideration, as follows.

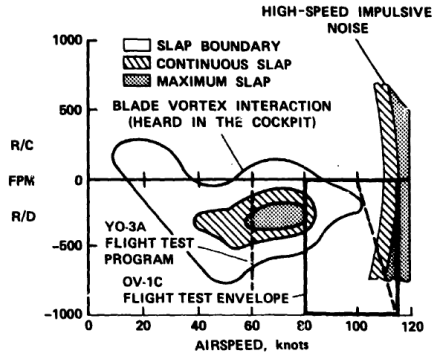

Figure 3 Impulsive noise boundaries for UH-1 series helicopter, from Schmitz et. al[18]

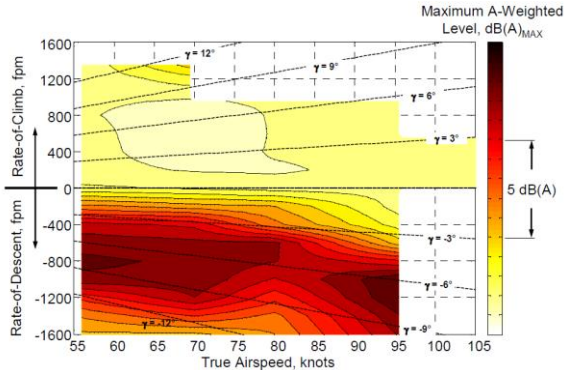

Figure 4- EC130 maximum A-weighted sound pressure level at centre microphone, from Gervais et al.[12]

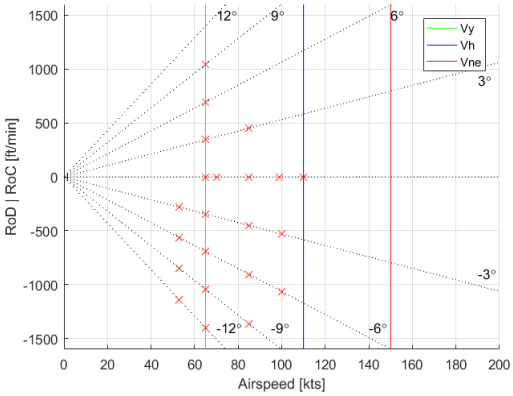

Figure 5 EC120 noise measurements points distribution in the flight envelope

Presented at 44th European Rotorcraft Forum, Delft, The Netherlands, 19-20 September, 2018

To allow variations in noise levels within a class, and do justice to the efforts done by manufacturers to make their helicopter models as silent as possible, an offset of hemisphere levels based on the difference (ΔL_{EPNL}) between registered certification levels[9] of the class reference and the helicopter type under consideration is applied. The noise level for a helicopter type in class i at flight condition j and emission angles φ and θ is then given by

$$L_{i,j}(f_c,\varphi,\theta) = \tilde{L}_h(f_c,\pm\varphi,\theta)_{i,j} + \Delta L_{EPNL} \quad (7)$$

where $\tilde{L}_h(f_c,\pm\varphi,\theta)_{i,j}$ is defined by eq. (4). The correction is applied to the overall hemisphere noise levels based on the difference in certification noise levels. For 'Chapter 8' certified helicopters, climb, level and descent conditions should be corrected based, respectively, on the take-off, overflight and approach certification levels.

Classes with more than one helicopter type are given in Table 3. Several helicopter type indicators are within brackets, e.g. [A600] in the R22 class, to indicate that the main/tail rotor configuration is mirrored with respect to the class reference. In this case the hemisphere azimuth angle has to be mirrored, hence the ± symbol in eq. (7).

In case no hemisphere set is available for a given helicopter class, a dedicated hemisphere set should be acquired by carrying out noise measurements. An intermediate solution is to temporarily group the helicopter type with a class for which a noise database is available. In this case certification noise levels are decisive and should be lower than or within the range of the target helicopter class. In case no certification noise levels are available or multiple classes can be selected based on this criterion, helicopter weight becomes the governing parameter. The class with the best matching weight that is still lower than the helicopter type considered is selected. ΔL_{EPNL} is set to zero to ensure a conservative estimate of noise levels.

4. PROPAGATION MODEL

A time delay is experienced between emission and reception of noise related to the time required for a sound wave to reach an observer. The relation between recorded time t_r and emitted time t_e is given by

$$t_r = t_e + \frac{r}{c} \quad (8)$$

where c is the speed of sound and r is the distance between helicopter and observer. At ICAO reference conditions (p_a=101325Pa, T=298.15K and h_{rel} =70%) the speed of sound is c=346.1m/s. To evaluate time integrated metrics, e.g. SEL or EPNL, it is required to express the predicted noise levels as a function of recorded time.

The total noise attenuation due to propagation

$$\Delta L_p = \Delta L_s + \Delta L_a + \Delta L_g \quad (9)$$

is governed by ground attenuation (ΔL_g), atmospheric attenuation (ΔL_a) and spherical spreading losses

$$\Delta L_s = -20\log_{10}\frac{r}{r_h} \quad (10)$$

where r_h=60m is the hemisphere reference distance. The contributions for ground attenuation and atmospheric attenuation will be addressed below.

4.1. Atmospheric attenuation

An unhindered propagating plane acoustic wave is still attenuated due to atmospheric absorption. This is caused by losses due to shear viscosity, thermal effects and molecular relaxation. These losses vary with temperature, pressure and in case of molecular (nitrogen and oxygen) relaxation losses, with humidity. They are also frequency dependent. A propagating plane wave attenuated by the atmosphere can be written as

$$p(t,s) = p_0 e^{-as} e^{i(\omega t - ks)} \quad (11)$$

where p is the pressure amplitude at a distance s, p_0 is the initial wave amplitude and a is the atmospheric attenuation in Nepers per m. This can be expressed in decibels by

$$\Delta L_{a,t}(f) = -20\log_{10}\frac{|p(t,s)|}{p_0} = -20\log_{10} e^{-as} = -\alpha(f)(r-r_h) \quad (12)$$

where α ($=20/\ln 10 \cdot a$) is the attenuation in dB/m.

The method described in SAE ARP5534[19] is followed to obtain α at ICAO reference conditions. The pure-tone mid-band attenuation coefficient given by

$$\alpha = 8.686 f^2 \left\{ 1.8556\cdot 10^{-11} + 6.6928\cdot 10^{-6}\cdot\frac{f_{rO}}{f_{rO}^2+f^2} + 1.3415\cdot 10^{-6}\cdot\frac{f_{rN}}{f_{rN}^2+f^2} \right\} \quad (13)$$

, where f is the pure-tone frequency of sound in Hz and the variables f_{rN}=75692Hz and f_{rO}=630.7Hz represent the vibrational relaxation frequencies of oxygen and nitrogen respectively.

Presented at 44th European Rotorcraft Forum, Delft, The Netherlands, 19-20 September, 2018

Table 5 Tabulated values of one-third octave band atmospheric attenuation per km propagation distance

f_c, Hz	ΔL_a/km, dB	f_c, Hz	ΔL_a/km, dB
10	0.0	400	2.3
12.5	0.0	500	3.1
16	0.0	630	4.1
20	0.0	800	5.2
25	0.0	1000	6.3
31.5	0.0	1250	7.5
40	0.0	1600	8.9
50	0.0	2000	10.6
63	0.1	2500	13.0
80	0.1	3150	16.6
100	0.2	4000	22.5
125	0.3	5000	31.0
160	0.5	6300	44.9
200	0.7	8000	67.6
250	1.1	10000	101.0
315	1.6		

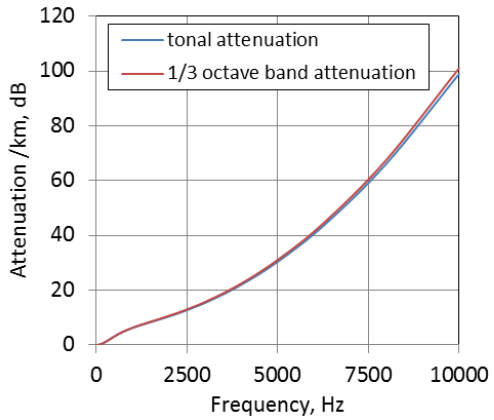

Figure 6 Tonal and one-third octave band atmospheric attenuation per km propagation distance

Eq. (13) gives the attenuation in dB/m for a pure-tone frequency. To infer the atmospheric attenuation for a one-third octave band the SAE method by Rickley et al.[20] is applied (see table 5 and figure 6).

4.2. Ground absorption

The solution[21,22,23] for a point source above an impedance surface is given by:

$$p(\mathbf{x}) = \frac{e^{ikr_1}}{r_1} + Q\frac{e^{ikr_2}}{r_2} \quad (14)$$

where p is the complex pressure amplitude, k the wavenumber, Q is the spherical reflection coefficient and r_1 and r_2 are the direct and reflected path length respectively. Assuming Q is approximately constant within a one-third octave band, the ground attenuation as function of centre frequency is given by[24]

$$\Delta L_g = 10\log\left\{1+\frac{r_1^2}{r_2^2}|Q|^2 + 2\frac{r_1}{r_2}|Q|I\right\} \quad (15)$$

, in which

$$I = \frac{\sin\left(0.727\, f_c \Delta R/c\right)}{0.727\, f_c \Delta R/c}\cos\left(6.325\, f_c \Delta R/c + \psi\right) \quad (16)$$

accounts for the interference patterns that occurs within a band. ΔR is the path length difference between the direct and reflected ray, c the speed of sound and ψ the argument of the spherical reflection coefficient. Equation (16) shows that in the high frequency limit, I tends to zero and eq. (15) reduces to a summation of two uncorrelated noise sources.

The spherical reflection coefficient Q is given by

$$Q = R_p + \left(1-R_p\right)F\left(d\right) \quad (17)$$

where

$$R_p = \frac{Z_s\cos\xi - 1}{Z_s\cos\xi + 1} \quad (18)$$

is the planar wave reflection coefficient. In the latter expression, Z_s is the surface impedance and ξ the angle of incidence of the incoming acoustic wave (0º corresponding to normal incidence). In eq.(16), F is a boundary loss factor, defined by

$$F\left(d\right) = 1 + id\sqrt{\pi}e^{-d^2}\,\mathrm{erfc}\left(-id\right) \quad (19)$$

which is a function of numerical distance

$$d = \frac{(1+i)}{2}\sqrt{kr_2}\left(\frac{1}{Z_s} + \cos\xi\right) \quad (20)$$

The complementary error function for complex arguments (erfc) is evaluated by numerical approximations[25,26].

The surface impedance Z_s is modelled by a single parameter model by Delaney and Bazley[27], which strikes a good balance between ease of use and accuracy. The surface is assumed locally reacting so that the surface impedance Z_s is equal to the specific normalized impedance of the ground medium. The surface impedance is then given by

$$Z_s = \left\{1 + 0.0511\left(\frac{f}{\sigma}\right)^{-0.754}\right\} + i\left\{0.0768\left(\frac{f}{\sigma}\right)^{-0.732}\right\} \quad (21)$$

The variables f and σ are, respectively, the frequency and the flow resistivity of the material.

Presented at 44th European Rotorcraft Forum, Delft, The Netherlands, 19-20 September, 2018

The recommended surface types are either concrete ($\sigma = 65 \cdot 10^6 Pa \cdot s / m^2$) for city areas or grass field ($\sigma = 200 \cdot 10^3 Pa \cdot s / m^2$) for rural areas. Other surface types are described in [24,27] and may be used when applicable.

5. VALIDATION OF THE METHOD

The new calculation method and the hemisphere databases were implemented in a software prototype NORAH[28] (NOise of Rotorcraft Assessed by a Hemisphere-approach) and used to validate the method. Validation is about confirmation that the end-product is in compliance with the given specifications and reporting of the full extent of performed validation activities go beyond the scope of this paper. Herein, we will limit ourselves to aspects relating to the evaluation of the model's accuracy.

5.1. Contour calculation

A SEL noise footprint for a take-off by a Robinson 22 was used as reference test case. The calculations were performed with both NORAH[28] and HELENA[12] using identical hemispheres. The flight path comprises (i) a hover section, (ii) a steep climb, (iii) a level flight section and (iv) a slow climb. The grid points covered a 2000 by 1000 m area enclosing the helicopter movement, with a grid resolution of 10 metres. The receiver height was 1.2 meter above soft ground. Figure 7 shows the footprints obtained by both methods, which are very similar - about 95% of all grid points yielded results within 1dB and 99.9% within 2dB. Potential reasons for the deviations could evolve from the fact that the proposed model has a slightly improved algorithm for atmospheric attenuation as well as from differences in the method for interpolation and extrapolation in the hemisphere.

5.2. Noise prediction versus measurement

A comparison was made of the NORAH's output with noise measurements, using a single hemisphere in the R22 set.

The first flight conditions considered was an 8.5º descent at 68kts airspeed. The data acquired in the test campaign – viz. the 4-fold noise measurements used to construct the hemisphere and the recorded flight paths – were used as input to the simulation. The latter becomes hence a loop-back control of the hemisphere, validating its integrity. Figure 8 shows the measured and predicted Sound Exposure Levels for a single run. Simulations for the repeat runs were used to estimate the prediction standard deviation, which is reflected in the error bars. The standard deviation varies between 1dB and 2dB, achieving its maximum where the noise levels are highest. The latter is in accordance with Olsman et al.[29] whom conclude that the largest spread in the SEL occurs at the location where the most intense BVI occurs.

A second case addressed a 6º descent at 82kts airspeed, for which the hemisphere was established based on a single measurement. The measured and predicted time histories of A-weighted overall sound pressure level (OASPL) and tonal corrected Perceived Noise Levels (PNLT) were compared – as shown in Figure 9 – and a good match was found. Compared to the slow weighted measurements, a more pronounced dip is found at $t_r = 18s$, suggesting that a higher directivity resolution is obtained for the predictions. This relates to the foundation of the hemispheres, which are derived from one-third octave band spectra sampled every 0.1s and as such describe the helicopter noise directivity with superior accuracy. The predicted EPNL and SEL values are within 0.3dB of the measured ones.

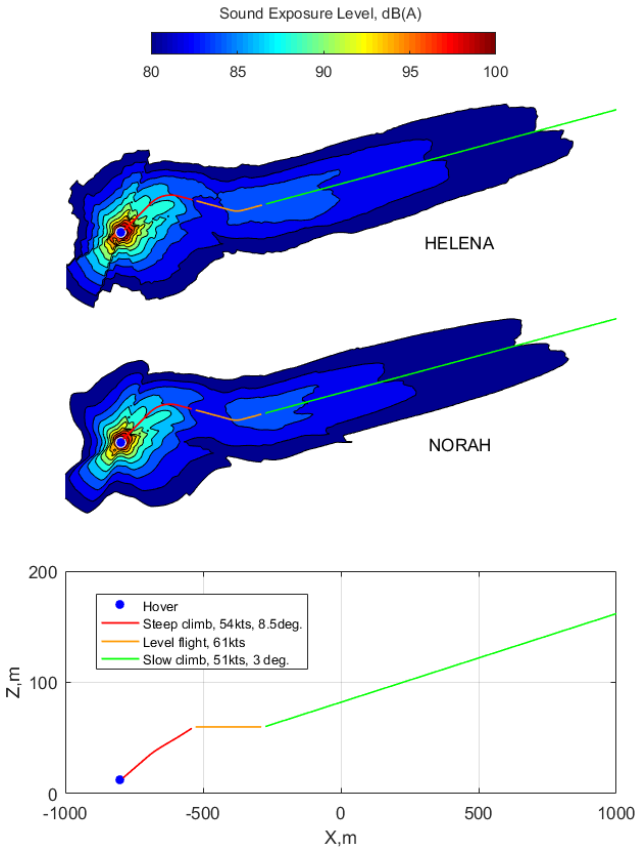

Figure 7 Top: SEL contour for HELENA, centre: SEL contour NORAH, bottom: track altitude profile

Presented at 44th European Rotorcraft Forum, Delft, The Netherlands, 19-20 September, 2018

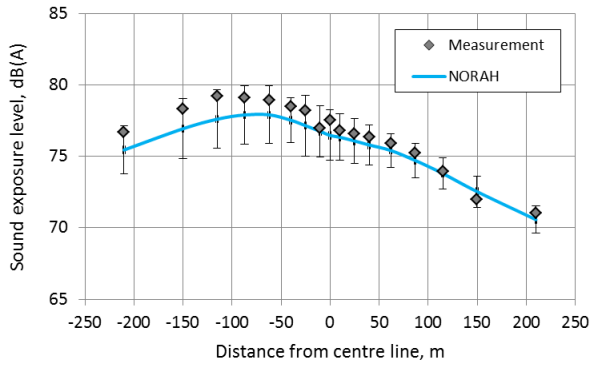

Figure 8 Comparison of sound exposure levels against simulated noise levels for 17 microphones, the error bars reflect the estimated standard deviation of the predictions

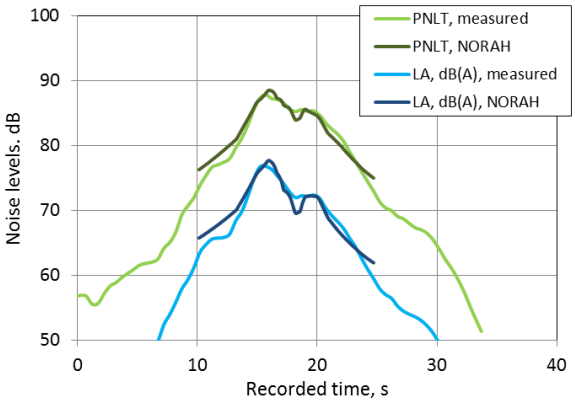

Figure 9 Time history of slow measured OASPL and PNLT compared to predicted noise levels

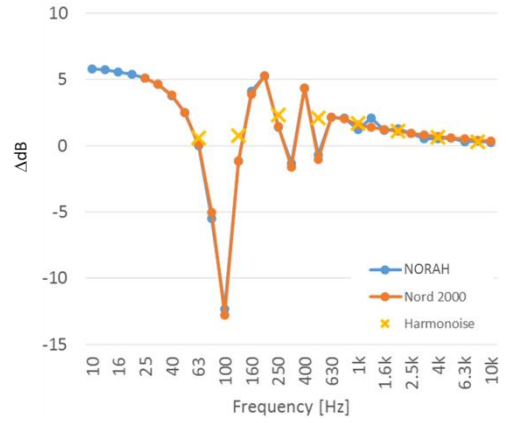

Figure 10 Comparison of ground attenuation predictions for the current method, Harmonoise and Nord 2000

5.3. Comparison with state-of-the-art propagation methods

Sound propagation losses comprise three terms; see eq. (9). The first reflects spherical spreading losses, is self-evident and needs no further validation. The second term is the atmospheric attenuation which refers to a public standard[19] hence requiring no further validation. The third term, ground attenuation, is further explored herein by definition of a reference test-case which includes comparison with Nord 2000[30] and Harmonoise[31]-based predictions. These methods represent the state-of-the-art for predicting outdoor sound propagation.

In the simulations, the source is assumed to be at 100 m above the ground. Soft ground is modelled with flow resistance equal to 200kPa s/m^2. The receiver is located at 1.2 m above the ground and 98.8 m ground distance, resulting in a 45 degrees elevation angle. The very good agreement of the current method compared to Nord 2000 and Harmonoise is shown in figure 10. Note that results for the latter method are given in octave bands as opposed to one-third octave bands.

6. CONCLUSIONS

A novel helicopter noise calculation method was defined that is suitable to support END monitoring activities.

Through a class representation approach the method is able to represent (more than) 70% of the European helicopter fleet based on noise databases that were obtained for 8 helicopter types.

Following a hemisphere approach, helicopter noise emission characteristics can be modelled with high fidelity, faithfully reproducing noise directivity and capturing noise sensitive conditions where e.g. Blade Vortex Interaction occurs.

The method is future proof, easily allowing the incorporation of new noise metrics when deemed required. For a given observer position and helicopter trajectory, the output of the method is 1/3 octave band spectra ranging from 10Hz to 10kHz as function of time. This enables to express results in Sound Exposure Level (SEL), Effective Perceived Noise Levels (EPNdB) or Maximum A-weighted Noise Levels (LA,max) but also apply new noise metrics.

The method matches ICAO Doc 9911 and ECAC Doc 29 in complexity and sophistication. The method description is short and simple and the implementation into software is straightforward. Computational resources requirements are limited and the input data and produced results are like that of aircraft noise models like ECAC Doc 29.

The method has been validated, by comparison against measurements and current state-of-the-art methods in helicopter noise modelling and propagation modelling. Notwithstanding this fact, the assumption that helicopters within a class possess comparative emission characteristics needs to be further scrutinized.

Presented at 44th European Rotorcraft Forum, Delft, The Netherlands, 19-20 September, 2018

ACKNOWLEDGEMENT

This work has been funded under the European Commission Service contract No. MOVE/C2/SER/2014-269/SI2.706115 for the development of a Public European Environmental Model Suite for Aviation.

REFERENCES

[1.] ECAC, 'Report on Standard Method of Computing Noise Contours around Civil Airports', ECAC Doc29, 4th Ed., 2016

[2.] M. Tuinstra, N. van Oosten and H. Olsen, 'The development of a European helicopter noise model', 44th European Rotorcraft forum, ERF-2018-50, 2018

[3.] Rotorspot Rotorcraft Registrations Database; http://www.rotorspot.nl

[4.] Aircraft Type Designators; ICAO Doc 8643, Edition 43; 14 April 2015; http://www.icao.int/publications/DOC8643/Pages/default.aspx

[5.] Jane's All the World's Aircraft; Jane's Information Group.

[6.] Various manufacturer's brochures, websites, etc.

[7.] EASA Type Certificate Data Sheets (TCDS); http://easa.europa.eu/document-library/type-certificates

[8.] FAA Type Certificate Data Sheets (TCDS); http://www.airweb.faa.gov/Regulatory_and_Guidance_Library/rgMakeModel.nsf/MainFrame?

[9.] EASA Noise Type Certificates Rotorcraft, Issue 21; 26 June 2015; https://easa.europa.eu/document-library/noise-type-certificates-approved-noise-levels

[10.] Luftfahrt-Bundesamt (German Federal Aviation Office) Noise Data, List 3: Helicopters; 15 June 2006; http://www.eacott.com.au/gallery/d/2060-1/Noise+Data+for+Helicopters.pdf

[11.] Canadian JHSAT Report 2000 accident data analysis; Canadian Joint Helicopter Safety Analysis Team Year 2000 Summary Report & Flight Hour Data Analysis; http://www.ihst.org/LinkClick.aspx?fileticket=5OAxM%2fS9IgE%3d&tabid=1507

[12.] M.Gervais, V. Gareton, A. Dummel and R. Heger, 'Validation of EC130 and EC135 environmental impact assessment using HELENA', American helicopter soc., 66th annual forum, Phoenix, 2010

[13.] J.A. Page, C. Wilmer, T. Schultz, K.J. Plotkin and J. Czech, 'Advanced Acoustic Model Technical Reference and User Manual', 2009

[14.] F. Guntzer, P. Spiegel and M. Lummer, 'Genetic optimization of EC-135 noise abatement flight procedures using an aeroacoustic database', 35th European rotorcraft forum, 2009

[15.] DOC 9501, Environmental technical manual on the use of procedures in the noise certification of aircraft, 3rd edition, 2004

[16.] M.Tuinstra, P.Sijtsma, 'Measurement of helicopter noise hemispheres utilizing a 100m vertical array', European Rotorcraft Forum 2012, Amsterdam, ERF-2012-019, 2012

[17.] R.W. Browne; Munt, R.M.; Simpson, C.R.; Williams, T.; Prediction of Helicopter Noise Contours for Land Use Planning, AIAA Paper 2004-2811, Manchester, UK, 2004

[18.] F.H. Schmitz and Y.H. Yu, 'Helicopter Impulsive Noise: Theoretical and Experimental Status', NASA TM 84390, 1984

[19.] SAE, 'Application of pure-tone atmospheric absorption losses to one-third octave-band data', ARP5534, 2013

[20.] E.J. Rickley, G.G. Flemming, C.J. Roof, 'Simplified procedure for computing the absorption of sound by the atmosphere', Noise Control Eng. J., Vol. 55, No.6, pp482-494, 2007

[21.] C.F. Chien and W.W. Soroka (1980), 'A note on the calculation of sound propagating along an impedance plane', J. Sound Vib., 69:340-343

[22.] C.F. Chien and W.W. Soroka (1976), 'Sound propagation along an impedance plane', J. Sound Vib., 43:9-20

[23.] X. Di and E. Gilbert (1993), 'An exact Laplace transform formulation for a point source above a ground surface', J. Acoust. Soc. Am., 93, 714-720

[24.] L.C. Sutherland and G.A. Daigle (1997), 'Encyclopedia of acoustics', chapter 32, pp341-365, ISBN 0-471-80465-7

[25.] M. Abramowitz and I.A. Stegun (1972), 'Handbook of mathematical functions with formula's, Graphs, and mathematical tables', Dover publications, inc., New York

[26.] F. Matta and A.R. Reichel (1971), 'Uniform computation of the error function and other related functions', Mathematics of Computation, 25, p.339-344

[27.] M.E. Delaney and E.N. Bazley (1970), 'Acoustic properties of fibrous absorbent materials', Appl. Acoust., Vol. 3, pp.105-116

[28.] N. van Oosten, L. Meliveo, M. Tuinstra, H. Olsen, 'The new EU helicopter noise model NORAH', 11th European Congress and Exposition on Noise Control Engineering, Euronoise, 2018

Presented at 44th European Rotorcraft Forum, Delft, The Netherlands, 19-20 September, 2018

[29.] W.F.J. Olsman and B.I. Schuchardt, 'Segmentwise Measurement of Helicopter Approach Noise with a Reduced Microphone Setup', Journal of the American Helicopter Society 60, 042005, 2015

[30.] B. Plovsing, Nord2000. Comprehensive Outdoor Sound Propagation Model. Part 2: Propagation in an Atmosphere with Refraction, DELTA Acoustics & Vibration, Report AV 1851/00 (revised), Hørsholm 2006

[31.] E. Salomons, D. van Maercke, J. Defrance, F. de Roo, 'The Harmonoise Sound Propagation Model', Acta Acustica, 2011

Presented at 44th European Rotorcraft Forum, Delft, The Netherlands, 19-20 September, 2018